Jahn–Teller energy dependence of Curie temperature in $La_{1-x}(Ca/Sr)_xMnO_3$

2006 J. Phys.: Condens. Matter 18 7851

(http://iopscience.iop.org/0953-8984/18/34/001)

INSTITUTE OF PHYSICS PUBLISHING JOURNAL OF PHYSICS: CONDENSED MATTER

J. Phys.: Condens. Matter **18** (2006) 7851–7862 doi:10.1088/0953-8984/18/34/001

Jahn–Teller energy dependence of Curie temperature in $La_{1-x}(Ca/Sr)_xMnO_3$

F L Tang and X Zhang

Laboratory of Advanced Materials, Department of Materials Science and Engineering, Tsinghua University, Beijing 100084, People's Republic of China

E-mail: xzzhang@tsinghua.edu.cn

Received 14 May 2006, in final form 27 June 2006
Published 7 August 2006
Online at stacks.iop.org/JPhysCM/18/7851

Abstract

Atomistic simulation has been performed on $La_{1-x}(Ca/Sr)_xMnO_3$ to investigate the change of Jahn–Teller energy E_{JT} and its quantitative dependence of the Curie temperature T_C. When the doping density x increases from 0 to 0.33 (0.25), it is found that E_{JT} of $La_{1-x}Ca_xMnO_3$ ($La_{1-x}Sr_xMnO_3$) decreases from 0.5 eV to 0.17 (0.1) eV. When the pressure changes from 0 to 4.5 GPa, E_{JT} of $La_{0.75}Ca_{0.25}MnO_3$ ($La_{0.89}Sr_{0.11}MnO_3$) decreases from 0.14 (0.18) eV to 0.07 (0.09) eV. With E_{JT} and estimated bandwidth W, we calculated T_C, which agrees well with experimental data, especially in the case of being under pressure. It is also found that about 75% enhancement of T_C is contributed by E_{JT} and the rest by W. Therefore, we propose that E_{JT} plays a main role, whereas W plays a much less but not negligible role on T_C.

1. Introduction

The manganese-based colossal magnetoresistive (CMR) oxides have been the subjects of intense investigations due to their rich underlying physics and potential application [1–5]. The close connection between the evolution of structural distortion and changes in the magnetotransport properties has been demonstrated, especially, proving that the local Jahn–Teller (JT) distortions have a dominant role for the localization of charge carriers [1, 2, 6].

For modern physics and chemistry, the Jahn–Teller effect is an important and fascinating phenomenon, because it provides a general method for understanding some properties of molecules and crystals and their origins [1, 7]. In manganites, the Jahn–Teller distortion of the MnO_6 octahedron lifts the double degeneracy in the e_g-orbitals [8]. In the 1960s, Kanamori [9] illustrated the Jahn–Teller effect within a simple mode: if a given electronic level of a cluster is degenerate in a structure of high symmetry, this structure is generally unstable, and this cluster will present a distortion toward a lower symmetry ionic arrangement. For Mn^{3+} ions in manganites, which are doubly degenerate in the undistorted crystal (the ideal simple perovskite structure), the degenerate e_g-orbital will be split by an energy (defined as

Jahn–Teller energy [10]) when the crystal is distorted. This distortion of the MnO_6 octahedron is 'cooperative' because once it occurs in a particular octahedron it will affect the neighbouring Mn^{3+} ions [1]. Following Kanamori, Millis [11] represented the two e_g-orbital states and Jahn–Teller energy using lattice and octahedral distortions in manganites.

Earlier studies have given many useful clues to the strong relation between the Jahn–Teller energy E_{JT} and Curie temperature T_C in doped manganites. Zhao *et al* [12] suggested that the giant oxygen isotope shift of T_C was very likely related to the JT polarization, which could play an important role in determining the electronic and magnetic properties in $La_{0.8}Ca_{0.2}MnO_{3+y}$. Then they proposed a formula $T_C \propto W_{eff} \propto W \exp(-\gamma E_{JT}/h\omega)$ to qualitatively explain the isotope effect on T_C merely with bandwidth W. Radaelli *et al* [13] believed that the E_{JT} influence on T_C in $A_{1-x}A'_xMnO_3$ cannot be ruled out, and a 20% change in E_{JT} will result in a comparable T_C variation. However, they found that the changes in E_{JT} induced by doping were very difficult to estimate because the information on the internal structural parameters was not available. From the comparison of T_C with W, they concluded that W was able to explain, at least qualitatively, the T_C variation upon doping or under pressure. With a formula similar to that given by Zhao *et al*, it was found that the high-temperature resistivity in $La_{0.9}Sr_{0.1}MnO_3$ can be well ascribed by the model of small-polaron hopping: T_C increased with decreasing JT polarization energy E_P (which can be estimated by the formula $E_P \approx 2E_A$, where E_A is the activation energy) [14]. The pressure and isotope effects on T_C in $La_{0.65}Ca_{0.35}MnO_3$ were also investigated with W and the formula given by Zhao *et al* [15].

Although the above work had given important insight to the E_{JT} dependence of the magnetic properties, especially of T_C, there are still some uncertainties to be considered. First, to our knowledge, the details of the change in E_{JT} of perovskite manganites upon doping or under pressure are lacking. Sometimes E_{JT} was estimated with E_A. Second, the quantitative E_{JT} dependence of T_C is needed, instead of a qualitative description. Finally, can W alone explain the change in T_C? This is puzzling because W is always changed by less than 10%, whereas T_C varies by more than a factor of two. In this paper, we focus on the variation of E_{JT} and its quantitative dependence of T_C in $La_{1-x}(Ca/Sr)_xMnO_3$ both upon doping and under pressure. For this purpose, systematic atomistic simulations were performed.

2. Simulation method

The crystal structure of a material at a given temperature and pressure can be predicted by minimizing its free energy. Our approach is to adjust the cell volume and atomic positions until the net pressure or stress is zero. The pressure P is simply the derivative of the free energy F with respect to volume V. Thus, for a cubic material,

$$P = \mathrm{d}F/\mathrm{d}V. \tag{1}$$

Calculating the free energy at a given volume and then recalculating it after making a small adjustment to the cell volume $\mathrm{d}V$ determines the pressure.

During the iterative procedure, a constant volume energy minimization is performed. Hence, each time the cell volume is modified; all atomic positions are adjusted so that they remain at a potential energy minimum. Thus by minimizing to constant pressure and including the vibrational component of the free energy, the crystal structure at a given temperature and pressure can be predicted.

Based on the widely used successful shell model [16] generalization of the Born model of a solid, the lattice energy E can be expressed as

$$E = \frac{1}{2}\sum_{i,j}\left[\frac{q_i q_j}{r_{ij}} + V(r_{ij})\right], \tag{2}$$

Table 1. Potential parameters for Sr^{2+} in $SrMnO_3$: short-range interaction and shell model parameters.

	Short-range interaction		
	A (eV)	ρ (Å)	C (eV Å^6)
Sr^{2+}–$O1^{2-}$	22 956.7020	0.2356	0.0
Sr^{2+}–$O2^{2-}$	40 452.3757	0.2252	0.0
Mn^{4+}–$O1^{2-}$	16 526.0604	0.2218	0.0
Mn^{4+}–$O2^{2-}$	16 741.0424	0.2217	0.0
$O1^{2-}$–$O1^{2-}$	22 764.3000	0.1490	43.0
$O2^{2-}$–$O2^{2-}$	22 764.3000	0.1490	43.0
$O1^{2-}$–$O2^{2-}$	22 764.3000	0.1490	43.0
	Shell-model parameters		
Species	Y (e)	K (eV Å^{-2})	
Sr^{2+}	1.831	21.53	
Mn^{4+}	4.000	95.0	
$O1^{2-}$	−2.389	42.0	
$O2^{2-}$	−2.389	42.0	

where the first item is the Coulombic energy introduced by long-range interactions of effective charges, and the second item is the short-range interactions. Short-range interaction is represented by a Buckingham potential:

$$V(r) = A\exp(-r/\rho) - Cr^{-6}, \tag{3}$$

where A, ρ, and C are fitting parameters. In order to describe the polarization of an individual ion and its dependence on the local atomic environment, it is treated by the core-shell model [16]. The interaction between the core and shell of any ion is treated as harmonic with a spring constant k and is represented by

$$E_v(d_i) = \tfrac{1}{2}kd_i^2, \tag{4}$$

where d_i is the relative displacement of core and shell of ion i. The polarization of a massless shell with charge Y and a core with charge X ($X + Y$ is the charge of the ion) can be calculated as

$$\alpha = \frac{Y^2}{k}, \tag{5}$$

where Y relates to the dielectric constant, and k is the force constant between core and shell, relating to the phonon frequency. Both parameters Y and k are fitting parameters.

This technique has been used for the simulation of many kinds of material [17–23]. Details of this technique are available in [24]. It should be stressed that the reliability of our simulation strongly depends on the validity of the potential model used, and the latter is assessed primarily by its ability to reproduce experimental crystal properties. The potential parameters used for $LaMnO_3$ and $CaMnO_3$ have been fitted, and they can reproduce the experimental crystal structure of $LaMnO_3$ and $CaMnO_3$ well, with the differences in lattice constants between the calculated and experimental data less than 1% [23]. The newly fitted potential parameters of $SrMnO_3$ are given in table 1. The differences in lattice constants and bond lengths of $SrMnO_3$ between calculated and experimental data are less than 0.001 Å.

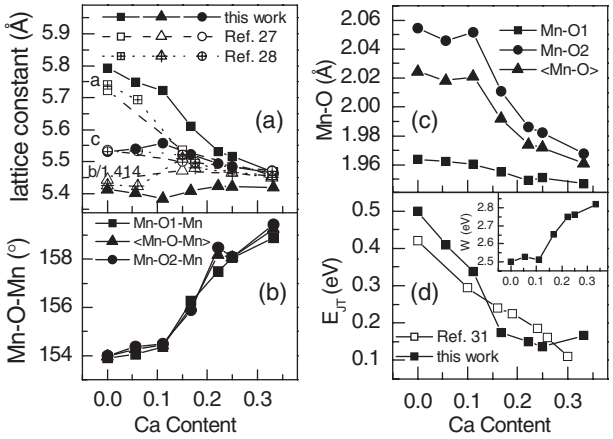

Figure 1. Lattice transitions in Ca-doped $LaMnO_3$ with doping content x: lattice constants (a), Mn–O–Mn angles (b), and Mn–O bond lengths (c). Changes in E_{JT} (d) and W (inset of (d)) with doping content x.

We have further examined the validity of our potential model of $LaMnO_3$ by calculating the pressure effect on the lattice constants of $LaMnO_3$ up to 3.4 GPa. The calculated compressibility is in agreement with the experimental value, indicating that the potentials we used can represent the crystal structure of $LaMnO_3$ [23]. We have investigated the vibrational contributions of Sr-doped $LaMnO_3$ at some low temperatures in order to further check the $SrMnO_3$ potential parameters. For studying the temperature effect on lattice constants and bond lengths, one converged configuration of $La_{0.833}Sr_{0.167}MnO_3$ was heated from 0 to 75 K. It was found that the lattice constants and Mn–O bond lengths are almost unchanged when temperature increases. This result is consistent with experimental results [25]. The vibrational check of Ca-doped $LaMnO_3$ was also done (<150 K) [23]. These vibrational checks indicate that our $SrMnO_3$ ($CaMnO_3$) potentials are stable and suitable in doped $LaMnO_3$ at low temperature less than 75 K (150 K). The above lattice, pressure, and temperature effect tests indicate that our potentials can represent the crystal structures of La (Ca, or Sr) MnO_3.

The size effect in simulation has also to be considered. For different sizes of supercells of $LaMnO_3$ containing 4 to 9 unit cells, the variation in lattice energy is less than 0.001 eV and the variation in lattice constants is less than 0.0001 Å. Therefore, the size effect can be neglected in our simulation. In this work, the initial structure for studying the doped $LaMnO_3$ is the crystallographic unit cell of $LaMnO_3$, which has four La^{3+} ions, four Mn^{3+} ions, four O1 ions and eight O2 ions. (In $LaMnO_3$, the oxygen ions in the La–O planes are denoted as O1, and the oxygen ions in the Mn–O planes are denoted as O2.) To meet the demand of number proportion of the Ca/Sr-doping ions, and make the calculations most efficient, the unit cell of $LaMnO_3$ is extended three times along both a-axis and c-axis directions. There are 36 La^{3+}, 36 Mn^{3+} and 108 O^{2-} ions in the extended supercell. For simulating the structure of $La_{1-x}(Ca/Sr)_xMnO_3$, $36x$ La^{3+} and $36x$ Mn^{3+} ions are substituted by Ca^{2+}/Sr^{2+} and Mn^{4+} ions, respectively.

3. Results and discussion

3.1. JT energy and JT distortion

For $La_{1-x}(Ca/Sr)_xMnO_3$, about 16 to 200 doping configurations have been simulated at every doping density. The average results are shown in figures 1 and 2. It is also noticed that the

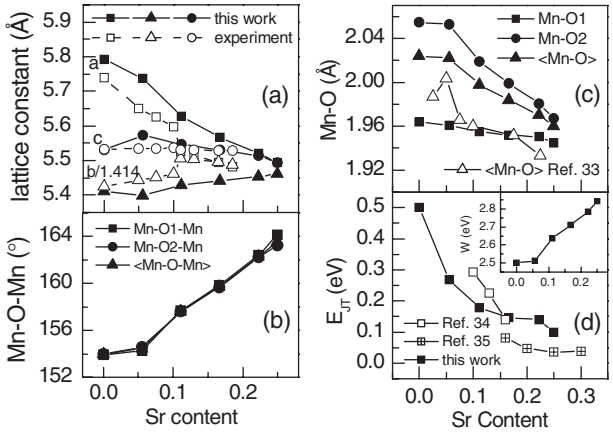

Figure 2. Lattice transitions in Sr-doped $LaMnO_3$ with doping content x: lattice constants (a), Mn–O–Mn angles (b), and Mn–O bond lengths (c). Changes in E_{JT} (d) and W (inset of (d)) with doping content x. In (a), experimental lattice constants are abstracted from [27] ($x = 0$) [32] ($x = 0.05$, 0.075 and 0.1), and [25] ($x = 0.11$, 0.13, 0.165 and 0.185).

converged configurations of $La_{1-x}(Ca/Sr)_xMnO_3$ always have the character of clustering or charge ordering ($x = 0.25$ or 0.33), i.e., Ca^{2+}/Sr^{2+} or Mn^{3+}/Mn^{4+} ions form clustering local structure or charge ordering stripes [1, 23, 26].

The variations of the lattice constants of $La_{1-x}Ca_xMnO_3$ ($0 \leqslant x \leqslant 0.33$) were calculated (figure 1(a)). It is found that as the doping content increases the calculated cell volume (not shown) decreases, lattice constant a decreases significantly, c decreases a little, but b increases somewhat. Our calculated cell volume and lattice constants agree with the experimental data [27, 28], indicating that our simulated structure can approximately represent the experimental doping structure.

Here we would like to make a remark. It is noted that our simulations were performed at 0 K whereas the experimental results were obtained from bulk or powder samples at higher temperatures [27, 28]. Can the calculated lattice constants correctly represent the experimental results? When the temperature increases from ∼0 to 300 K, the cell volume of $La_{1-x}Ca_xMnO_3$ ($x = 0.06$, 0.15, 0.25, and 0.33) [28] increases on average by ∼1.2 $Å^3$, but the change in cell volume due to Ca-doping ($x = 0$ to 0.33) [27, 28] was ∼13 $Å^3$, about ten times larger than that caused by temperature. In comparison with the doping effect, the temperature effect on lattice constants is very small and can be neglected. Therefore, our simulated data can describe the experimental structural change.

The changes of MnO_6 octahedra were also calculated: as the doping density increases from 0 to 0.33, the Mn–O–Mn bond angle increases from 154° to 159° (figure 1(b)), the Mn–O2 bond length decreases, and the Mn–O1 bond length decreases a little (figure 1(c)). The difference between Mn–O bond lengths decreases, indicating a reduction in MnO_6 octahedral (JT) distortion.

Taking into account only lattice distortions, the cooperative Jahn–Teller energy E_{JT} can be presented using the following formula [29]:

$$\frac{E_{JT}}{N_{Mn}} = -\frac{1}{2}\sqrt{\frac{3}{2}}\lambda\left[\sqrt{(Q_{2u}+Q_{2s})^2+(Q_{3u}+Q_{3s})^2}+\sqrt{(Q_{2u}-Q_{2s})^2+(Q_{3u}-Q_{3s})^2}\right], \tag{6}$$

where N_{Mn} is the number of Mn ions in the lattice, and λ is the Jahn–Teller coupling constant. In equation (6),

$$Q_{2u} = \frac{a_0}{\sqrt{2}}(e_{xx} - e_{yy}), \tag{7}$$

$$Q_{3u} = \frac{a_0}{\sqrt{6}}(2e_{zz} - e_{xx} - e_{yy}), \tag{8}$$

$$Q_{2s} = \frac{a_0}{\sqrt{2}}(v_{sx} - v_{sy}), \tag{9}$$

$$Q_{3s} = \frac{a_0}{\sqrt{6}}(2v_{sz} - v_{sx} - v_{sy}), \tag{10}$$

where a_0 is the lattice parameter of the ideal cubic perovskite structure ($N_{\mathrm{Mn}} = 1$). In this work $a_0 = (abc/4)^{1/3}$ as our simulated structure has symmetry $Pnma$. In equations (7) and (8), e_{jj} is the diagonal component of the conventional strain tensor referred to the ideal cubic perovskite lattice. In equations (9) and (10) $v_i^a = u_i^a - u_{i-\hat{a}}^a$, where u_i^a and $u_{i-\hat{a}}^a$ are displacements of the two O ions in the MnO_6 octahedron along the a-direction. Details of the formulae can be found in [1] and [29]. The Jahn–Teller distortion Q of an octahedron is defined as

$$Q = \sqrt{(Q_{2u} + Q_{2s})^2 + (Q_{3u} + Q_{3s})^2} + \sqrt{(Q_{2u} - Q_{2s})^2 + (Q_{3u} - Q_{3s})^2}, \tag{11}$$

where Q_{2s} and Q_{3s} can be easily calculated from the coordinates of six O atoms, and Q_{2u}, Q_{3u} from lattice parameters. The Jahn–Teller distortion of a configuration is calculated by averaging the Q of every octahedron in the superlattice. The Q at a specific doping level is calculated by averaging the Q of every configuration considered.

Using simulated lattice constants and structural data of MnO_6 octahedra at every doping density, the change in E_{JT} of $La_{1-x}Ca_xMnO_3$ can be calculated. Using equation (6) and simulated structural data, we calculated E_{JT} of Ca-doped $LaMnO_3$, which decreases from 0.5 eV (E_{JT} of $LaMnO_3$ is ~0.5 eV) [30] to 0.17 eV (figure 1(d)) as the doping density increases from 0 to 0.33.

It was found that E_{JT} could also be estimated using experimental E_{A} by the formulae $E_{\mathrm{JT}} \approx E_{\mathrm{P}}$ [12] and $E_{\mathrm{P}} \approx 2E_{\mathrm{A}}$ [14]. This estimated E_{JT} is called the deduced E_{JT} in this paper. Teresa *et al* [31] calculated E_{JT} as a function of Mn^{4+} content in $La_{0.7}Ca_{0.3}MnO_{3-\delta}$ using E_{A}. If one considers the Mn^{4+} content as the doping density, their E_{JT} can be compared with our results (figure 1(d)). Our calculated E_{JT} of $La_{1-x}Ca_xMnO_3$ ($0 \leqslant x \leqslant 0.25$) has a similar magnitude and variation as the results given by Teresa *et al* (figure 1(d)).

For Sr-doping, the calculated lattice constants (figure 2(a)) also approximately agree with the experimental data [25, 27, 32]. As the doping density increases from 0 to 0.25, the Mn–O–Mn angle increases from 154° to 164° (figure 2(b)), the Mn–O2 bond length decreases, and the Mn–O1 bond length decreases a little (figure 2(c)). The calculated average Mn–O bond length is consistent with the experimental value [33]. The decreasing difference between Mn–O bond lengths indicates a reduction of octahedral distortion. Our calculated E_{JT} decreases from 0.5 to 0.1 eV, which has a similar magnitude and variation as the deduced E_{JT} [34, 35] (figure 2(d)), indicating that our result is reliable.

We studied the pressure ($\leqslant$4.5 GPa) effect by using one converged configuration of $La_{0.75}Ca_{0.25}MnO_3$ and $La_{0.89}Sr_{0.11}MnO_3$. The simulated results are shown in figure 3. For $La_{0.75}Ca_{0.25}MnO_3$, as the pressure increases from 0 to 4.5 GPa, the Mn–O–Mn angle increases from 157.5° to 159° (figure 3(a)), the Mn–O2 bond length decreases, and the Mn–O1 bond length remains almost unchanged. Our calculated average Mn–O bond length agrees well with the experimental value [36] (figure 3(b)). One can find that as the pressure

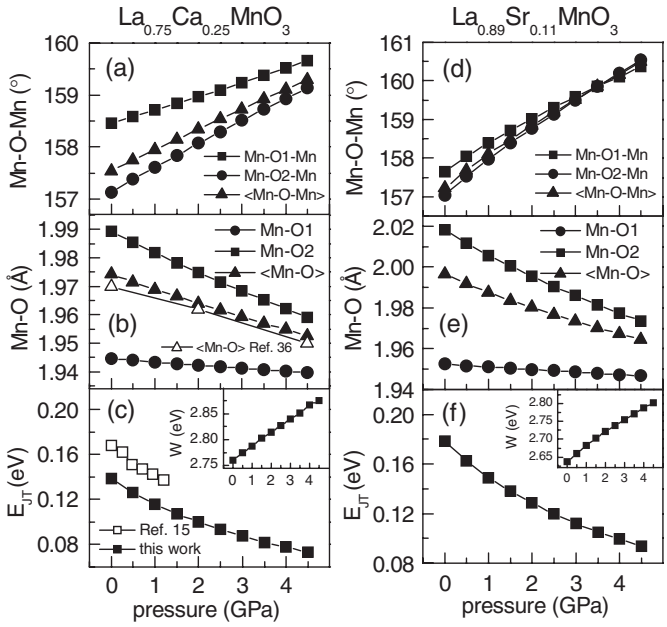

Figure 3. Changes of $La_{0.75}Ca_{0.25}MnO_3$ under pressure: Mn–O–Mn angles (a), Mn–O bond lengths (b), E_{JT} (c) and W (inset of (c)). Changes of $La_{0.89}Sr_{0.11}MnO_3$ under pressure: Mn–O–Mn angles (d), Mn–O bond lengths (e), E_{JT} (f) and W (inset of (f)).

increases from 0 to 4.5 GPa the difference between Mn–O bond lengths decreases, indicating a reduction of MnO_6 octahedral distortion. Correspondingly, E_{JT} (figure 3(c)) decreases from 0.14 to 0.07 eV. The deduced E_{JT} [15] of $La_{0.65}Ca_{0.35}MnO_3$ has the same variation as our calculated E_{JT} when the pressure is less than 1.2 GPa. For $La_{0.89}Sr_{0.11}MnO_3$, as the pressure increases from 0 to 4.5 GPa, the Mn–O–Mn angle increases from 157° to 160° (figure 3(d)), the Mn–O2 bond length decreases, the Mn–O1 bond length remains almost unchanged (figure 3(e)), and the calculated E_{JT} (figure 3(f)) decreases from 0.18 to 0.09 eV.

Upon doping or under pressure, MnO_6 octahedra in doped $LaMnO_3$ manifest interesting distortions. With increasing Ca/Sr-doping density, a MnO_6 octahedron will undergo at least three types of movement: contraction in volume, rotation to its position of ideal perovskite structure, and movement of the inner Mn ion from the centre of the octahedron. Under increasing pressure, the octahedron will also contract in volume and rotate to its position of the ideal perovskite structure, but the inner Mn ion will return slightly to the centre. It seems that the last type of movement of MnO_6 octahedra has not been reported. These changes in octahedra of doped $LaMnO_3$ will influence the Mn–O bond and Mn–O–Mn angle, and thus change E_{JT} and W.

For a $Mn^{3+}O_6$ octahedron in doped $LaMnO_3$, the JT distortion in it remains, but is somewhat smaller than that in undoped $LaMnO_3$. For a $Mn^{4+}O_6$ octahedron in doped $LaMnO_3$, its distortion is very small but larger than that (almost zero) in $CaMnO_3$. These differences in octahedral distortions may arise from the different local structure between $La_{1-x}(Ca/Sr)_xMnO_3$, $LaMnO_3$, and $Ca(Sr)MnO_3$. In addition, we suppose the reduction in E_{JT} of doped $LaMnO_3$ arises from two aspects: the reduction of Mn^{3+} number [31] and the lesser distortion of $Mn^{3+}O_6$ compared with that in undoped $LaMnO_3$.

3.2. Curie temperature

To calculate T_C, we first estimated the change of W in doped $LaMnO_3$ with an empirical formula

$$W = k\frac{\cos\delta}{d^{3.5}}, \tag{12}$$

where k is a proportional constant, δ is the tilt angle defined as $(180-\phi)/2$, ϕ is the Mn–O–Mn angle, and d is the Mn–O bond length. This empirical relation, a straightforward result from the tight-binding approximation [13], has been proved effective for doped manganites [13, 14, 22, 37–44]. With the Mn–O length and Mn–O–Mn angle of $LaMnO_3$ (figure 1, at $x = 0$) and $W = 2.5$ eV [45], we can obtain the coefficient $k = 30.3$ eV in equation (12). With the Mn–O length and Mn–O–Mn angle in figure 1 (figures 2 or 3) and equation (12), we calculated W at other doping densities or under pressure, and show it in the inset of figure 1(d) (figure 2(d), 3(c), or 3(f)).

The formula for T_C, given by Zhao *et al* [12] from the small polaron theory, can be rewritten as

$$T_C = BW\exp(-\gamma E_{JT}/h\omega), \tag{13}$$

where B is a proportional constant, ω is a characteristic frequency of the optical phonons depending on the oxygen isotope mass M ($\omega \propto M^{-1/2}$), and γ is a dimensionless parameter as a function of E_{JT}/W. γ decreases when E_{JT}/W decreases and has a value of $0 < \gamma \leqslant 1$. Small polaron theory suggested that the numerical constant γ depends on the range of the electron–phonon interaction alone [46]. Equation (13) has been used for conductors, and has proved suitable for CMR materials [12–15, 31, 37, 47, 48].

To use equation (13), first, we have to estimate the value of $h\omega$. For undoped $LaMnO_3$, the value of $h\omega$ is ~0.075 eV [30]. Because light doping of Ca or Sr could not cause much mass variation, we simply selected $h\omega = 0.075$ eV for all doping densities under study. We then estimated γ. Since γ decreases when E_{JT}/W decreases, we assume

$$\gamma = \alpha E_{JT}/W, \tag{14}$$

where α is a proportional constant. Using the experimental T_C, as well as calculated W, and E_{JT} at a certain doping density, one can select suitable γ and B in equation (13) as a starting point of T_C calculation. With equation (14), γ, W, and E_{JT} at this doping density, α is obtained. With equation (14), α, W, and E_{JT} at other doping densities, γ at other densities is obtained. Finally, with γ, W, and E_{JT} at other doping densities, the corresponding T_C can be calculated using equation (13).

When the Ca/Sr-doping density x is less than ~0.08, the doped $LaMnO_3$ is an insulating antiferromagnet, and does not undergo a ferromagnetic to paramagnetic phase transition [1]. When $x \geqslant 0.08$, the doped $LaMnO_3$ undergoes a ferromagnetic to paramagnetic phase transition at T_C. For Ca-doping, we used $T_C \approx 120$ K (at $x = 0.06$), $B = 105$ K, $\gamma = 0.17$, W and E_{JT} shown in figure 1(d) to calculate T_C (figure 4(a)). It is found that T_C first increases when $0.06 \leqslant x < 0.25$, saturates when $x = 0.25$ and then seemingly decreases a little when $x \leqslant 0.33$. For Sr-doping, we used $T_C \approx 135$ K (at $x = 0.06$), $B = 139$ K, $\gamma = 0.5$, W, and E_{JT} shown in figure 2(d) to calculate T_C (figure 4(b)). T_C increases more quickly than that of Ca-doping when $0.06 \leqslant x \leqslant 0.25$. The calculated and experimental [1, 49–52] T_C of $La_{1-x}(Ca/Sr)_xMnO_3$ have a similar variation as a function of x. The difference between them may arise from two aspects: the proportional assumption of equation (14) and the initial selection of $h\omega = 0.075$ eV.

We calculated the T_C of $La_{0.75}Ca_{0.25}MnO_3$ under pressure with $T_C \approx 220$ K (at 0 GPa), $B = 99$ K, $\gamma = 0.11$, W and E_{JT} shown in figure 3(c). It is found that T_C (figure 4(c)) increases

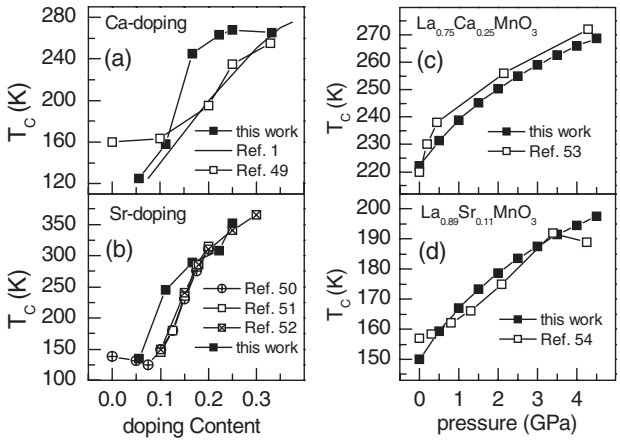

Figure 4. Variation of T_C of Ca-doped (a) and Sr-doped (b) $LaMnO_3$ with doping content x. Variation of T_C of $La_{0.75}Ca_{0.25}MnO_3$ (c) and $La_{0.89}Sr_{0.11}MnO_3$ (d) under pressure.

gradually from 220 K to ∼270 K when the pressure increases from 0 to 4.5 GPa. Our calculated T_C agrees very well with the experimental results [53] (figure 4(c)). For $La_{0.89}Sr_{0.11}MnO_3$, we took $T_C \approx 150$ K (at 0 GPa), $B = 76$ K, $\gamma = 0.11$, W, and E_{JT} in figure 3(f) to calculate T_C. When the pressure increases from 0 to 4.5 GPa, T_C (figure 4(d)) increases gradually from 150 K to ∼200 K. The calculated T_C also agrees well with the experimental results [49]. For $La_{0.75}Ca_{0.25}MnO_3$ and $La_{0.89}Sr_{0.11}MnO_3$, pressure has similar effect: E_{JT} decreases by ∼50%; $\delta T_C/\delta P$, the difference of T_C with respect to pressure is ∼10 K GPa^{-1}, consistent with some experimental results (10 K GPa^{-1} [15], 11 K GPa^{-1} [53], and 8 K GPa^{-1} [54]).

Now we study the E_{JT} and W dependence of T_C using the total differential of T_C with respect to E_{JT} and W. Using equation (14), equation (13) can be rewritten as

$$T_C = BW\exp(-\beta E_{JT}^2/W), \tag{15}$$

where $\beta = \alpha/h\omega$. If E_{JT} and W are independent of each other, the total differential of T_C can be expressed as

$$\Delta T_C = \frac{\partial T_C}{\partial W}\Delta W + \frac{\partial T_C}{\partial E_{JT}}\Delta E_{JT}, \tag{16}$$

where

$$\frac{\partial T_C}{\partial W} = B\left(1+\beta\frac{E_{JT}^2}{W}\right)\exp\left(-\beta\frac{E_{JT}^2}{W}\right), \tag{17}$$

and

$$\frac{\partial T_C}{\partial E_{JT}} = -2B\beta E_{JT}\exp\left(-\beta\frac{E_{JT}^2}{W}\right). \tag{18}$$

Using equations (17), (18), and calculated E_{JT} and W, we obtained the average $\frac{\partial T_C}{\partial W}$ and $\frac{\partial T_C}{\partial E_{JT}}$. Thus, $\frac{\partial T_C}{\partial W}\Delta W$, the change of T_C due to the change of W, and $\frac{\partial T_C}{\partial E_{JT}}\Delta E_{JT}$, the change of T_C due to the change of E_{JT}, are obtained. In the case of Ca/Sr-doping, the enhancement of T_C due to E_{JT} is 76% (80%) and that due to W is 24% (20%). In the case of $La_{0.75}Ca_{0.25}MnO_3$ ($La_{0.89}Sr_{0.11}MnO_3$) under pressure, the enhancement of T_C due to E_{JT} is 76% (73%) and that due to W is 24% (27%). These results indicate that E_{JT} plays a main role, whereas W plays a much less but not negligible role on T_C. Our result is in qualitative agreement with the suspicion

proposed by Radaelli *et al* [13] that 20% variation of E_{JT} may introduce a comparable T_C variation. It is also noted that if the enhancement of T_C due to W (which changes by ∼12% upon doping or ∼5% under pressure) is estimated just using equation (13) without consideration of E_{JT}, the result is only ∼12% (doping) or ∼5% (pressure), which is significantly underestimated compared with the result estimated using equation (15). Hence, using bandwidth alone is not sufficient to describe the change in T_C.

From our simulation, we can illustrate such a physical scenario in doped manganites: when different cations are doped into manganites or under pressure, both their lattice distortion and MnO_6 octahedral distortion (JT distortion for $Mn^{3+}O_6$) will reduce. On the one hand, these structural transitions can lead to different e_g electron hopping integrals by the mechanism of double exchange, i.e., the bandwidth W is changed. On the other hand, doping leads to local structural transition, for example, the JT polaron distortion energy E_{JT} (relating to the strength of the electron–phonon couple) is changed. Then, magnetic properties, such as T_C, can be changed by the changes in W and E_{JT}.

Though the quantitative relation between E_{JT}, W, and T_C has been discussed with simulated structural data, we do not exclude other factors affecting T_C by changing the value of B and/or γ in equation (13). For example, $\delta T_C/\delta x$, the difference in T_C (calculated value in figures 4(a) and (b)) with respect to the doping density x, is obtained: ∼500 K for Ca-doping ($0.06 \leqslant x \leqslant 0.33$) and ∼1100 K for Sr-doping ($0.06 \leqslant x \leqslant 0.25$); the latter is about twice the former. Nevertheless, the corresponding value of $\delta E_{JT}/\delta x$ (the difference in E_{JT} with respect to the doping density x; E_{JT} can be found in figures 1(d) and 2(d)) is −0.87 eV for Ca-doping and −0.84 eV for Sr-doping; the latter is almost equal to the former. At the same time, $\delta W/\delta x$ (the difference in W with respect to the doping density x; W can be found in insets of figures 1(d) and 2(d)) is 1.1 eV for Ca-doping and 1.7 eV for Sr-doping; the latter is larger than the former by about 50%. The change in E_{JT} or W is smaller than the change in T_C upon doping. In addition, in equation (13), the choice of γ for Ca-doping (0.17) is much smaller than that for Sr-doping (0.5). The choice of B for Ca-doping (105 K) is also different from that for Sr-doping (139 K). We believe that there are some other factors affecting γ and B, and then affecting T_C, apart from E_{JT} and W. We suppose that different local crystal and electronic structures, introduced by different doping ions, such as Ca^{2+} and Sr^{2+}, lead to such great T_C difference. This could mean that a more sophisticated model would be necessary to elucidate these factors.

4. Conclusion

We have performed systemic atomistic simulation on $LaMnO_3$ upon Ca/Sr-doping and on $La_{0.75}Ca_{0.25}MnO_3$ ($La_{0.89}Sr_{0.11}MnO_3$) under pressure. The change in Jahn–Teller energy E_{JT} and its quantitative dependence of Curie temperature T_C were investigated. On increasing x from 0 to 0.33 (0.25), it was found that E_{JT} in $La_{1-x}Ca_xMnO_3$ ($La_{1-x}Sr_xMnO_3$) decreases from 0.5 eV to 0.17 (0.1) eV. Under pressure from 0 to 4.5 GPa, E_{JT} in $La_{0.75}Ca_{0.25}MnO_3$ ($La_{0.89}Sr_{0.11}MnO_3$) decreases from 0.14 (0.18) eV to 0.07 (0.09) eV. Calculated and deduced E_{JT} are similar in magnitude and variation. With E_{JT} and estimated bandwidth W, we calculated T_C of Ca/Sr-doped manganites, which agree well with experimental results, especially in the case of being under pressure. We also found that ∼75% enhancement of T_C is contributed by E_{JT} and ∼25% by W. Therefore, we propose that E_{JT} plays a more important role than W, and W alone is not sufficient to quantitatively describe the change in T_C.

Upon doping, MnO_6 octahedra in $La_{1-x}(Ca/Sr)_xMnO_3$ will contract in volume, rotate to their positions of ideal perovskite structure, and the Mn ions will move from the centres of the

octahedra. Under pressure, MnO_6 octahedra in $La_{0.75}Ca_{0.25}MnO_3$ and $La_{0.89}Sr_{0.11}MnO_3$ will also contract and rotate, but the Mn ions will return slightly to the centres of the octahedra.

Acknowledgments

The authors would like to thank the Ministry of Science and Technology of China (Grant Nos TG2000067108 and 2002CB613500) and National Science Foundation of China (Grant No. 90401013) for financial support. The authors would also like to thank Shao Yang for his work in fitting the potential parameters of $SrMnO_3$.

References

[1] Dagotto E, Hotta T and Moreo A 2001 *Phys. Rep.* **344** 1
[2] Salamon M B and Jaime M 2001 *Rev. Mod. Phys.* **73** 583
[3] Haghiri-Gosnet A-M and Renard J-P 2003 *J. Phys. D: Appl. Phys.* **36** R127
[4] Hwang H Y, Cheong S-W, Radaelli P G, Marezio M and Batlogg B 1995 *Phys. Rev. Lett.* **75** 914
[5] Fontcuberta J, Martínez B, Seffar A, Piñol S, García-Muñoz J L and Obradors X 1996 *Phys. Rev. Lett.* **76** 1122
[6] Ramirez A P 1997 *J. Phys.: Condens. Matter* **9** 8171
[7] Bersuker I B 2006 *The Jahn–Teller Effect* (Cambridge: Cambridge University Press)
[8] Jahn H A and Teller E 1937 *Proc. R. Soc.* A **161** 220
[9] Kanamori J 1960 *J. Appl. Phys.* **31** 14S
[10] Millis A J 1998 *Science* **392** 147
[11] Millis A J 1996 *Phys. Rev.* B **53** 8434
[12] Zhao G-M, Conder K, Keller H and Müller K A 1996 *Nature* **381** 676
[13] Radaelli P G, Iannone G, Marezio M, Hwang H Y, Cheong S-W, Jorgensen J D and Argyriou D N 1997 *Phys. Rev.* B **56** 8265
[14] Chen X J, Soltan S, Zhang H and Habermeier H-U 2002 *Phys. Rev.* B **65** 174402
[15] Lorenz B, Heilman A K, Wang Y S, Xue Y Y, Chu C W, Zhang G and Franck J 2001 *Phys. Rev.* B **63** 144405
[16] Dick B G and Overhauser A W 1958 *Phys. Rev.* **112** 90
[17] Catlow C R A, Thomas J M, Parker S C and Jefferson D A 1982 *Nature* **295** 658
[18] Catlow C R A and Price G D 1990 *Nature* **347** 243
[19] Zhang X and Catlow C R A 1993 *Phys. Rev.* B **47** 5315
[20] Zhang X, Yip K W and Ong C K 1995 *Phys. Rev.* B **51** 1277
[21] Bourova E, Parker S C and Richet P 2000 *Phys. Rev.* B **62** 12052
[22] Tang F L and Zhang X 2005 *J. Phys.: Condens. Matter* **17** 6507
[23] Tang F L and Zhang X 2006 *Phys. Rev.* B **73** 144401
[24] Gale J and Rohl A L 2003 *Mol. Simul.* **29** 291
[25] Dabrowski B, Xiong X, Bukowski Z, Dybzinski R, Klamut P W, Siewenie J E, Chmaissem O, Shaffer J, Kimball C W, Jorgensen J D and Short S 1999 *Phys. Rev.* B **60** 7006
[26] Shibata T, Bunker B, Mitchell J F and Schiffer P 2002 *Phys. Rev. Lett.* **88** 207205
[27] Subías G, García J, Blasco J and Proietti M G 1998 *Phys. Rev.* B **57** 748
[28] Huang Q, Santoro A, Lynn J W, Erwin R W, Borchers J A, Peng J L, Ghosh K and Greene R L 1998 *Phys. Rev.* B **58** 2684
[29] Ahn K H and Millis A J 2001 *Phys. Rev.* B **64** 115103
[30] Ramakrishnan T V, Krishnamurthy H R, Hassan S R and Pai G V 2004 *Phys. Rev. Lett.* **92** 157203
[31] Teresa J M D, Dörr K, Müller K H, Schultz L and Chakalova R I 1998 *Phys. Rev.* B **58** R5928
[32] Chatterji T, Ouladdiaf B, Mandal P, Bandyopadhyay B and Ghosh B 2002 *Phys. Rev.* B **66** 54403
[33] Shibata T, Bunker B A and Mitchell J F 2003 *Phys. Rev.* B **68** 24103
[34] Anane A, Dupas C, Dang K L, Renard J P, Veillet P, Guevara A M D L, Millot F, Pinsard L and Revcolevschi A 1995 *J. Phys.: Condens. Matter* **7** 7015
[35] Bhattacharya D, Chakraborty A and Maiti H S 1999 *J. Phys.: Condens. Matter* **11** 5845
[36] Meneghini C, Levy D, Mobilio S, Ortolani M, Nuñez-Reguero M, Kumar A and Sarma D D 2001 *Phys. Rev.* B **65** 12111
[37] Moritomo Y, Murakami K, Ishikawa H, Hanawa M, Nakamura A and Ohoyama K 2004 *Phys. Rev.* B **69** 212407
[38] Medarde M, Mesot J, Lacorre P, Rosenkranz S, Fischer P and Gobrecht K 1995 *Phys. Rev.* B **52** 9248

[39] Pinsard-Gaudart L, Rodríguez-Carvajal J, Daoud-Aladine A, Goncharenko I, Medarde M, Smith R I and Revcolevschi A 2001 *Phys. Rev.* B **64** 64426
[40] Chang C F, Chou P H, Tsay H L, Weng S S, Chatterjee S, Yang H D, Liu R S, Shen C H and Li W-H 1998 *Phys. Rev.* B **58** 12224
[41] Cui C and Tyson T A 2004 *Appl. Phys. Lett.* **84** 942
[42] Arularj A, Santhosh P N, Gopalan R S, Guha A, Raychaudhuri A K, Kumar N and Rao C N R 1998 *J. Phys.: Condens. Matter* **10** 8497
[43] Kozlenko D P, Glazkov V P, Jirák Z and Savenko B N 2003 *J. Magn. Magn. Mater.* **267** 120
[44] Kozlenko D P, Glazkov V P, Sadykov R A, Savenko B N, Voronin V I and Medvedeva I V 2003 *J. Magn. Magn. Mater.* **258/259** 290
[45] Millis A J, Littlewood P B and Shraiman B I 1995 *Phys. Rev. Lett.* **74** 5144
[46] Alexandrov A S 2000 *Phys. Rev.* B **61** 12315
[47] Fontcuberta J, Laukhin V and Obradors X 1999 *Phys. Rev.* B **60** 6266
[48] Ausloos M, Hubert L, Dorbolo S, Gilabert A and Cloots R 2002 *Phys. Rev.* B **66** 174436
[49] Schiffer P, Ramirez A P, Bao W and Cheong S-W 1995 *Phys. Rev. Lett.* **75** 3336
[50] Paraskevopoulos M, Mayr F, Hemberger J, Loidl A, Heichele R, Maurer D, Müller V, Mukhin A A and Balbashov A M 2000 *J. Phys.: Condens. Matter* **12** 3993
[51] Mandal P and Ghosh B 2003 *Phys. Rev.* B **68** 14422
[52] Urushibara A, Moritomo Y, Arima T, Asamitsu A, Kido G and Tokura Y 1995 *Phys. Rev.* B **51** 14103
[53] Postorino P, Congeduti A, Dore P, Sacchetti A, Gorelli F, Ulivi L, Kumar A and Sarma D D 2003 *Phys. Rev. Lett.* **91** 175501
[54] Tissen V G, Ponyatovskii E G, Nefedova M V, Laukhin V, Martínez B, Fontcuberta J, Arsenov A A and Mukovskii Y M 2000 *J. Magn. Magn. Mater.* **211** 145